Supplementary Information

A Laser-Driven Optical Atomizer: Photothermal Generation and Transport of Zeptoliter-Droplets along a Carbon Nanotube Deposited Hollow Optical Fiber

Hyeonwoo Lee,[a] Mikko Partanen,[a,b] Mingyu Lee,[a] Sunghoon Jeong,[a] Hyeung Joo Lee,[a] Kwanpyo Kim,[c,d] Wonhyoung Ryu,*[e] Kishan Dholakia,*[a,f] and Kyunghwan Oh*[a]

[a]*Photonic Device Physics Laboratory, Department of Physics, Yonsei University, 50 Yonsei-ro, Seodaemun-gu, Seoul 03722, Korea. E-mail: koh@yonsei.ac.kr*

[b]*Photonics Group, Department of Electronics and Nanoengineering, Aalto University, P.O. Box 13500, 00076 Aalto, Finland*

[c]*Department of Physics, Yonsei University, Seoul 03722, Korea*

[d]*Center for Nanomedicine, Institute for Basic Science (IBS), Seoul 03722, Korea*

[e]*Biomedical and Energy System Laboratory, Department of Mechanical Engineering, Yonsei University, 50 Yonsei-ro, Seodaemun-gu, Seoul 03722, Korea. E-mail: whryu@yonsei.ac.kr*

[f]*SUPA, School of Physics and Astronomy, University of St. Andrews, KY16 9SS, UK. E-mail: kd1@st-andrews.ac.uk*

- Numerical analyses of the droplet transport

Trajectories of individual droplets ejected from an atomizer have been of great interest in fluidic studies because they determine how far the droplets would travel in the longitudinal and transverse directions, defining the transport range. Our all-fiber optical atomizer showed a unique droplet transport pattern, as shown in Fig. 2(c–f), forming a spherical propagation front. To understand its mechanism, we conducted numerical analyses using a commercial finite element method package, COMSOL multiphysics. We assumed that the thermomechanical forces acting on the nanodroplets are thermophoretic force ($\vec{F}_{ther}$) originating from the temperature gradient, drag force ($\vec{F}_{drag}$) from the air convection, and gravitational force ($\vec{F}_{g}$). Hence, the net force ($\vec{F}_{net}$) exerting on a particle having the velocity $\vec{v}$ with the diameter d, mass m, and thermal conductivity k is expressed as[S1, S2]

$$\vec{F}_{net} = \vec{F}_{ther} + \vec{F}_{drag} + \vec{F}_{g} = -\frac{6\pi d k \mu^2 C_s \vec{\nabla} T}{\rho(2k_{air} + k)T} + 3\mu\pi d(\vec{u} - \vec{v}) - m\vec{g} \tag{S1}$$

where μ is the viscosity of air, ρ is the density of air, $\vec{u}$ is the velocity of air, C_s is the dimensionless number 1.17, k_{air} is the thermal conductivity of air, T is the temperature distribution, and $\vec{g}$ is the gravitational acceleration. The Navier–Stokes equation and heat equation solver in COMSOL was used to calculate the velocity and temperature fields of air. Note that we did not include the effects of radiation pressure on individual nanodroplets in the analyses to isolate them from the thermomechanical contributions in simulations.

We chose an axially symmetric model since our optical atomizer had a cylindrical shape. In simulations, we set a cross-sectional plane with a width of 218.75 μm and a height of 500 μm that included the HOF segment near the output end, as shown in Fig. S1(a). We assumed a ring-shaped microheater as in the experimental SWCNTs thin film over HOF. Numerical simulations for the temperature distribution, velocity field of air, and droplet trajectories with the diameter of *d* = 66 nm, corresponding to the smallest volume ~150 zl in Fig. 3(h), are summarized in the supplementary information, Movie S1–S3, respectively. The optical atomizer in the movie is located on the top left. The droplets are transported downward from the fiber end facet and then rise upward by the convection, which is qualitatively consistent with experimental observations, as shown in Fig. 2(c–f). We further traced the droplets' trajectories as they exited from the fiber facet at various radial positions in Fig S1(b). The simulation results are consistent with the experimental droplet distribution in Fig. 2(c–f). As the further trajectory was not possible to trace because of the resolution limit of our optical microscope, in Fig. S1(b), we plotted the experimental measurement of the spherical droplet distribution near the fiber end facet represented in Fig. 2(e). The farthest position in our simulation with the same order of magnitude shows a droplet distribution similar to our observations using the high-speed camera.

We further conducted parametrical analyses by varying physical quantities. The results are summarized in Fig. S2. First, we numerically analyzed the mass flow rate (MFR) and longitudinal transport distance (LTD) as a function of the absorbed laser power, P_L. See Fig. S2(a). Both MFR and LTD showed a linear increase with P_L. At P_L= 19 mW, our measured experimental value, we numerically estimated MFR and LTD to be 211 ng/s and 247 µm, respectively. Note that LTD of 300 µm in experiments in Fig. 2e is consistent with the theoretical estimation. Furthermore, we numerically calculated LTD as a function of droplet diameter, and the results are shown in Fig. S2(b) at MFR = 211 ng/s. We obtained that LTD was nearly constant irrespective of the droplet diameter. This is attributed to the equilibrium among the three components in the net force of the above Equation S1. Consequently, the droplets ejected from the end of the optical atomizer form a uniform spherical front in the air, as illustrated in Fig. 2(c–f).

Although the simulations in Fig. S1, 2 agree qualitatively with experiments in Figs. 2(c–f), the difference between them is attributed to two factors that we did not include in the thermomechanical simulations. First, we did not include the effects of the air pressure in the HOF depicted in Fig. 1(a). Since the liquid would thermally expand by the microheater at the output end, the liquid will result in a compressive pressure to the air trapped in HOF, contributing to the ejection of liquid droplets. Second, we did not consider the light pressure exerted by the incident laser. The light emanating from the atomizer forms a light cone defined by the effective numerical aperture of glycerol-filled HOF, contributing to droplet transport in the air. Accurate numerical analyses, including these effects, are beyond the scope of this report, and further numerical investigation is being pursued by the authors.

- Vapor pressure for liquid ejection

We further investigated the effect of vapor pressure on atomization. Using the experimental conditions of the ejection initiating time t_i = 16.6 ms for 19.0 mW absorbed laser power in Table 1, we estimated the temperature of the liquid to be 75℃. We inferred this value from Movie S1, a solution to the heat equation, where the temporal response of the maximum temperature of glycerol is presented in Fig. S3(a). Considering the pressure at the fluid interface inside the capillary, which is well-known as the Young–Laplace equation, the vapor pressure p_{vapor} of the liquid with surface tension σ for optical atomization can be predicted as the following equation where the geometry is presented in the inset of Fig. S3(b).[S3]

$$p_{capillary} = 2\sigma cos\theta / R_{hole} < p_{vapor}(t_i) \quad \text{(S2)}$$

However, referring to the temperature at t_i = 16.6 ms as 75℃ in Fig. S3(a), the corresponding pressure of glycerol for the atomization is estimated at 0.004 kPa in Fig. S3(b). Additionally, the liquid whose vapor pressure is higher than 0.004 kPa at room temperature, such as pure water and ethanol, cannot be loaded in this system since the capillary pressure cannot prevent its spontaneous evaporation. Thus, to apply such materials in an optical atomizer, their vapor pressure should be reduced by dissolving dyes or adding other liquids, such as glycerol or fatty acid.

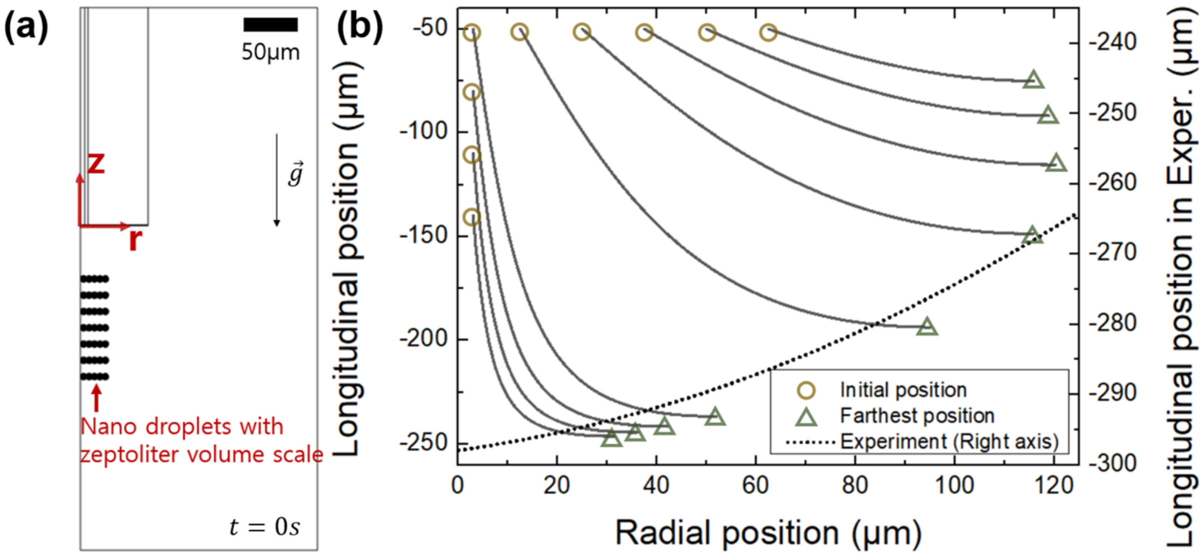

Fig S1. (a) Diagram of the initial position of the droplets for numerical analysis. The left vertical axis corresponds to the axis of the rotational symmetry. (b) The initial and farthest positions of the droplets in Movie S3 and the experimental measurement of the spherical front in Fig. 2(e).

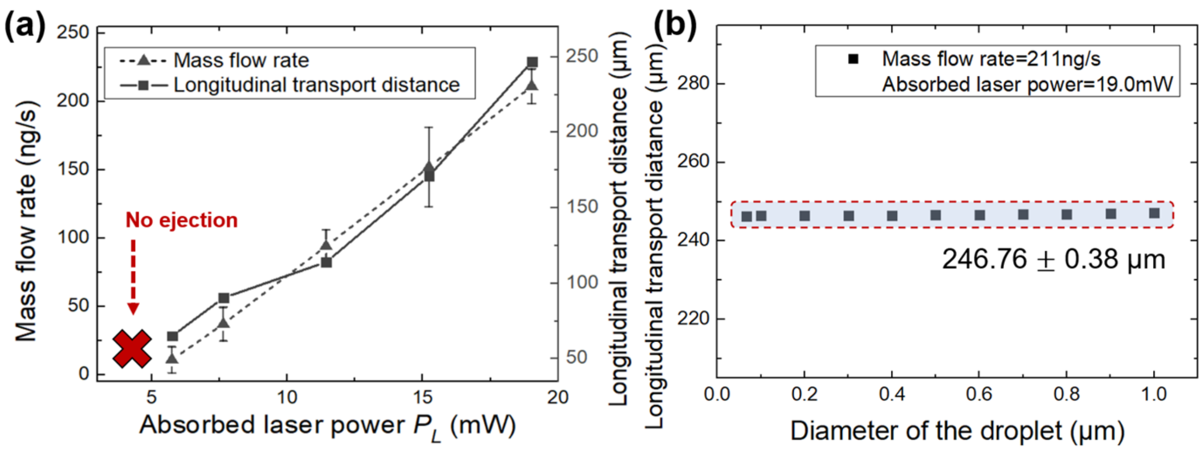

Fig. S2. (a) Simulation results for longitudinal transport distance (LTD) and mass flow rate (MFR) at various absorbed laser power. (b) The LTD as a function of the diameter of the droplet. Here, we set the absorbed laser power to 19 mW and MFR to 211 ng/s, estimated from (a).

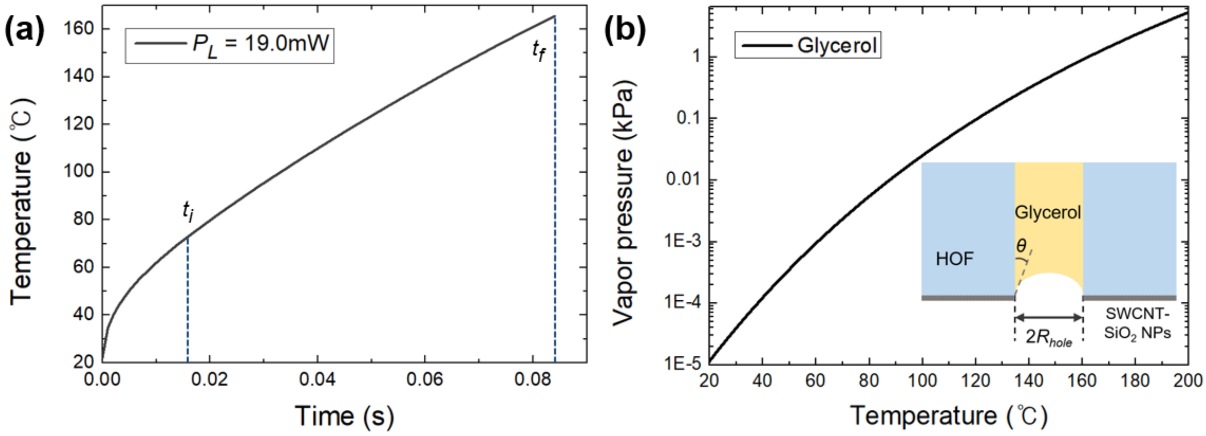

Fig. S3. (a) Maximum temperature of glycerol as a function of the time. (b) Vapor pressure of glycerol as a function of the temperature, provided by the reference[S4]. The inset shows the geometry of the optical atomizer, where θ is the contact angle of the glycerol inside the HOF hole with its radius R_{hole}.

References

S1. L. Mädler and S. K. Friedlander, *Aerosol Air Qual. Res.*, 2007, **7**, 304-342.

S2. K. J. Laidler, J. H. Meiser and B. Sanctuary, *Physical chemistry*, 1982.

S3. D. B. Asay, M. P. De Boer and S. H. Kim, *J. Adhes. Sci. Technol.*, 2010, **24**, 2363-2382.

S4. Chemical Engineering and Materials Research Information Center (CHERIC), https://www.cheric.org/research/kdb/hcprop/showcoef.php?cmpid=912&prop=PVP (Accessed November 2021).